INTERNATIONAL SOCIETY FOR
SOIL MECHANICS AND
GEOTECHNICAL ENGINEERING

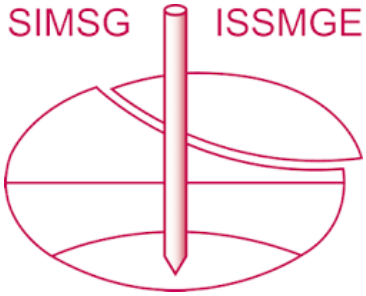

This paper was downloaded from the Online Library of the International Society for Soil Mechanics and Geotechnical Engineering (ISSMGE). The library is available here:

https://www.issmge.org/publications/online-library

This is an open-access database that archives thousands of papers published under the Auspices of the ISSMGE and maintained by the Innovation and Development Committee of ISSMGE.

5ICEGE
5th International Conference on Earthquake Geotechnical Engineering
January 2011, 10-13 | Santiago, Chile
Paper No. NRFLO

NORMAL AND REVERSE FAULT RUPTURE INTERACTION WITH CAISSON FOUNDATIONS: CENTRIFUGE MODELLING AND NUMERICAL SIMULATION

Marianna LOLI [1], Ioannis ANASTASOPOULOS [2], Fraser M. BRANSBY [3], George GAZETAS [4]

ABSTRACT

Permanent ground displacements due to faulting constitute a secondary, yet not less destructive, earthquake associated hazard, in addition to shaking. In fact, a great variety of structures suffered extensive deformation loading, and even failed, when crossed by the outcropping fault rupture in recent large magnitude earthquakes. Owing to their rigidity, caisson foundations are believed to be less sensitive to fault induced loading compared to other foundation types. This paper investigates experimentally and numerically the response of a caisson foundation subjected to dip slip (normal and reverse) fault rupture. A series of centrifuge tests were conducted to explore the mechanisms of fault rupture–caisson interaction, focusing on the effect of the caisson position with reference to the free field fault outcrop. The fault rupture was found to develop preferentially around the margins of the rigid caisson body, which acted as a kinematic constrain, altering sometimes dramatically the free field rupture pattern. Depending on the caisson position, the fault diverted towards the hanging wall or the footwall side of the caisson, or bifurcated, spreading the soil failure at a wider area on both sides. 3-D nonlinear numerical simulation of the problem was also developed and validated through comparison with the experimental results. A further numerical parametric investigation was finally carried out, showing the strong effect of the exact caisson position on the response of the system.

Keywords: Fault Rupture; Centrifuge modeling; Numerical modeling; Caisson Foundations.

INTRODUCTION

Faults, although being the generation source of earthquakes, were traditionally given little attention by the engineering community. The devastating earthquakes of 1999 in Turkey and Taiwan, however, came to prove that surface fault ruptures can be a significant hazard for structures and highlighted the need to develop design methods and guidelines against faulting-induced loading. A variety of structures were crossed by the surface fault rupture during the Kocaeli (Turkey, 1999) and Chi-Chi (Taiwan, 1999) earthquakes and a significant number of field case histories has been reported in the literature [e.g. Youd et al., 2000; Chang et al., 2000; Dong et al., 2003; Pamuk et al., 2005; Faccioli et al., 2008].

Several studies have considered the response of a structural system interacting with a propagating fault

[1] MSc, National Technical University of Athens, e-mail: mariannaloli@yahoo.com.
[2] Adjunct Lecturer, National Technical University of Athens, e-mail: ianast@civil.ntua.gr.
[3] Senior Lecturer, University of Dundee, e-mail: m.f.bransby@dundee.ac.uk.
[4] Professor, National Technical University of Athens, e-mail: gazetas@ath.forthnet.gr.

rupture, revealing that the presence of a structure may alter, sometimes dramatically, the free field rupture path. The mechanics of this phenomenon, termed Fault Rupture–Soil–Foundation–Structure Interaction (FR–SFSI), have been analyzed on the basis of : interpretation of real case histories [Anastasopoulos & Gazetas, 2007] ; centrifuge experiments [Bransby et al., 2008; Ahmed & Bransby, 2009] ; and numerical analyses [e.g. Paolucci & Yilmaz, 2008; Anastasopoulos et al., 2008; 2009].

Aiming to extend the research work on the mechanisms of FR–SFSI, which is currently (more or less) limited to the response of shallow foundations, this paper investigates the interaction of deep embedded foundations (caissons) with a rupturing normal and reverse fault. A combination of centrifuge model testing and numerical simulation of the problem was employed to this end. A series of centrifuge experiments were carried out to investigate the response of the caisson foundation, concentrating on the effects of its position relative to the fault. After validating the effectiveness of the numerical analysis methodology against experimental results, a parametric study was conducted to offer additional insight into the effect of the exact foundation position. Different interaction mechanisms, taking place for different caisson positions, are identified and the consequent system response is discussed.

PROBLEM DEFINITION AND METHODOLOGY

Figure 1 illustrates schematically the main features of the studied problem (indicatively for the case of reverse fault rupture) and defines the Cartesian coordinate system adopted. A 5 x 5 x 10 (m) square in plan caisson foundation is considered, supported on a 15 m thick layer of dense ($D_r \approx 80\%$) dry sand. It carries a total vertical load of approximately 20 MN, which represents the weight of a superstructure of significant size (e.g., a medium span bridge). Reverse and normal (upwards and downwards) fault displacement of vertical amplitude h (throw) is applied at the bedrock. The displaced block of soil (i.e. the hanging wall) moves upwards with a dip angle of 60°, whereas the footwall remains stationary. The fault deformation forces the caisson to move as a rigid body, experiencing both translational δ and rotational θ displacements.

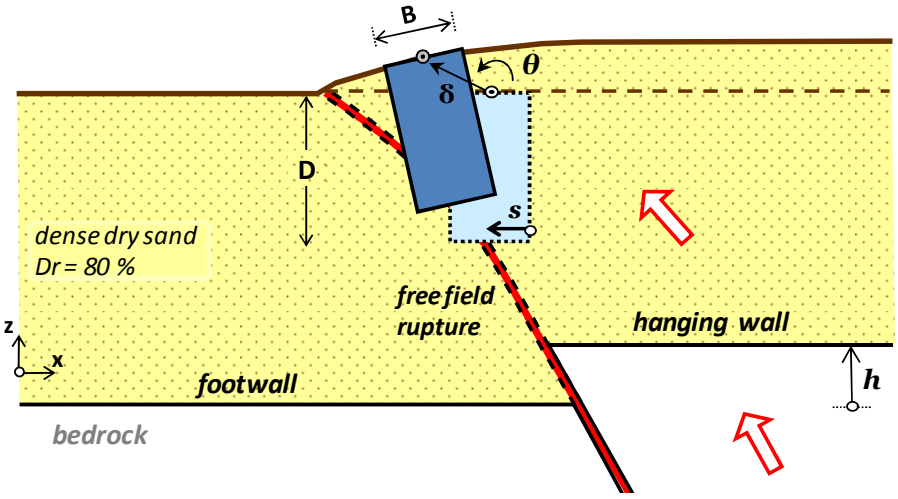

Figure 1. **Schematic illustration of the studied problem for the case of reverse fault rupture.**

Centrifuge Testing

A series of 8 in total centrifuge model tests were conducted in the beam centrifuge of the University of Dundee at an operational acceleration of 100 g. The experimental study aimed at investigating the mechanisms taking place for different positions of the caisson with reference to the fault. This is expressed by parameter *s*, which is defined as the distance between the caisson right corner and the point that the free field fault rupture would cross the foundation base (Figure 1). For each type of fault rupture (thrust/normal) a series of 3 fault rupture–caisson interaction tests were conducted, wherein the caisson was placed at different positions relative to the fault *s/B*, along with an additional free field test, which was used to determine the fault rupture trace in the free field (in absence of the foundation). Table 1 outlines the centrifuge testing program.

A photograph of the centrifuge model inside the strongbox is shown in Figure 2a, as deformed after completion of test ML-05, where the caisson was placed at a position $s/B = 0.22$. The 150 mm deep (i.e. 15 m at prototype scale) soil layer was prepared by dry air pluviation of Fontainebleau sand [Gaudin, 2002]. The sand was pluviated from a specific height with a fixed sieve aperture to control the mass flow rate, giving a uniform density $D_r \approx 80\%$ ($\gamma = 16.11$ kN/m^3). Direct shear tests were conducted to investigate the soil stress–strain and volumetric behaviour. For a mean value of relative soil density $D_r = 80\%$, the peak and residual friction angles of the soil were measured as $\varphi_{peak} = 37°$ and $\varphi_{res} = 31°$ at a normal effective stress representative of the middle of the soil depth (i.e. $\sigma'_v = 120$ kPa for depth $z = -7.5$ m). The dilation angle ψ was measured as approximately 10° for the same representative normal stress.

The caisson model was made of steel, having a total mass of 1.025 kg (corresponding to a prototype of 2050 Mg). Aiming to have realistically rough soil–caisson interfaces, the caisson model sides were needle-gunned (except the side that faced the Perspex window of the strongbox). The frictional properties at the caisson-soil interface were measured through direct-shear tests performed on similar needle-gunned steel specimens, which gave a friction angle of 19.8° at peak and 17° at residual conditions.

Table 1. Centrifuge testing program.

CENTRIFUGE TESTS			
Reverse Faults		*Normal Faults*	
Test	*Description*	*Test*	*Description*
WA-01		ML-06	
ML-04	s/B = -0.78	ML-08	s/B = 0.28
ML-05	s/B = 0.22	ML-10	s/B = 0.58
ML-03	s/B = 0.62	ML-07	s/B = 0.78

The faulting process was simulated using a split box, the moving part of which is made to translate using a hydraulic actuator. Fault deformation was applied during spinning at 100 g in a controllable, progressive, quasi-static manner reaching base dislocations of around 3.5 m (at prototype scale). A digital camera was used to take pictures of the model from a fixed position inside the centrifuge "*gondola*". Approximately 100 pictures per test were taken at progressively increasing fault displacements. The photographic data were then analyzed using the Geo-PIV programme, written by White et al. [2003], to calculate caisson displacements and the shear strains developed within the soil.

Finite Element Modelling

Numerical simulations of the centrifuge model tests were performed employing the finite element (FE) method, using the ABAQUS code. The model dimensions were chosen to be the same as the dimensions of the physical model at prototype scale. Finite element modelling of strain localization, in conjunction with strain–softening constitutive modeling, may lead to mesh-dependency problems associated with the inherent limitation of the FE method in reproducing shear band formation and propagation within granular materials. More specifically, since the width of the FE shear band will be equal to the element size (d_{FE}), ideally d_{FE} should be equal to the width of the real shear band d_B ($\approx 16d_{50}$ for sand, or $N\,x\,16d_{50}$ to model centrifuge test results). However, practically this might only be implemented when modeling laboratory-scale experiments. In general, due to computation time limitations, the FE shear "band" will always be substantially thicker than the real one. In this study, following the results of sensitivity analysis with respect to FE mesh refinement [Anastasopoulos et al., 2007 and Loli et al., 2010], an element width d_{FE} = 0.5 m was selected as a reasonable compromise between accuracy and computational effectiveness.

Figure 2b shows the deformed FE mesh for s/B = 0.22, for comparison with the physical model (Figure 2a). It is noted that only half of the model was simulated, taking advantage of symmetry along the centre-line of the foundation (which corresponds to the location of the Perspex front face in the centrifuge models).

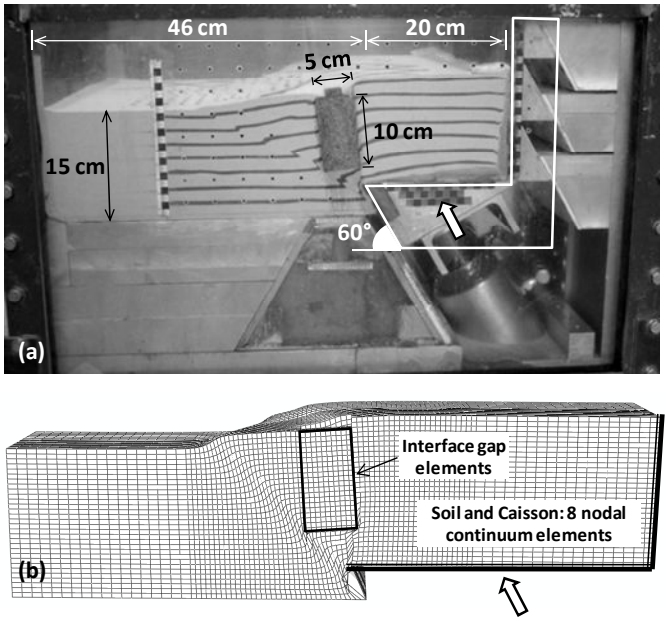

Figure 2. **Combined experimental and numerical study : (a) photo of the faulting apparatus and the centrifuge model (for reverse fault rupturing) ; (b) snapshot of deformed FE mesh.**

Soil was modeled with hexahedral continuum finite elements. The elasto-plastic constitutive relation described by Anastasopoulos et al. [2007] was used and encoded in ABAQUS through a user subroutine. This assumes elastic pre-yield soil behaviour defined by the secant shear modulus G_s, which was increased linearly with soil depth. The Mohr–Coulomb failure criterion was used to define failure accompanied by an isotropic strain softening law, which degraded the friction (φ) and dilation (ψ) angles linearly with octahedral plastic shear strain γ^{pl}_{oct}, according to the following relationships:

$$\varphi ; \psi = \begin{cases} \varphi_p - \frac{\varphi_p - \varphi_{res}}{\gamma_f^p} \gamma_{oct}^p \; ; \psi_p \left(1 - \frac{\gamma_{oct}^p}{\gamma_f^p}\right) & , for \; 0 \le \gamma_{oct}^p < \gamma_f^p \\ \varphi_{res} \; ; \; \psi_{res} = 0 & , for \; \gamma_{oct}^p \ge \gamma_f^p \end{cases} \quad (1)$$

where : φ_p and φ_{cs} the peak and critical state soil friction angles; ψ_p the peak dilation angle; and $\gamma_f{}^{pl}$ the octahedral plastic shear strain at the end of softening.

3-D continuum elements were also used for the caisson, which was assumed to be linearly elastic with typical stiffness properties for steel. The soil–caisson interface was modeled using contact elements (to allow sliding and/or detachment (assuming hard contact pressure-overclosure conditions) to occur. In order to simulate the centrifuge experiments, the interface properties were calibrated to match the frictional properties of the steel–sand interface as measured in the direct shear tests.

CHARACTERISTIC RESULTS – VALIDATION OF NUMERICAL METHOD

Due to space limitations, results are presented in detail only for two of the fault rupture–caisson interaction tests, one for each type of tectonic movement, and compared with the numerical analysis to illustrate the effectiveness of the numerical method. Yet, the mechanisms of fault rupture–caisson interaction for all the studied caisson positions (Table 1) as well as the free field response to reverse and normal fault rupture have been comprehensively reported in Loli et al. [2010 a and b].

Reverse Fault Rupture at s/B = 0.28 (Test ML-08)
In this test, the caisson was positioned so that the free field rupture would cross the caisson base 1.1 m to the left of its right corner (s = 0.28 B). As expected the rigid caisson mass interacts with the rupturing fault modifying significantly the failure pattern in comparison to the free field path. The mechanisms of fault–caisson interaction are highlighted in Figure 3.

Figure 3a shows a set of images captured at different – characteristic time points during faulting. Significant soil deformation can be observed for h = 0.8 m propagating vertically towards the soil surface on the right (hanging wall) side of the caisson and causing significant sliding to take place along the right caisson sidewall (indicated by the dotted line), yet without evident fault plane formation (see also corresponding shear strain contours in Figure 3b, as deduced through image analysis of the test results). However, after 0.7 m of additional fault displacement (h = 1.5 m) a localization plane (*F1*) has clearly formed and propagated from the base dislocation point to the right corner of the foundation and all along its right sidewall.

At the same time, a secondary localization (*F2*) appears. Initiating from the bedrock dislocation, *F2* intersects with the left (footwall) caisson base corner propagating with a much shallower dip angle. Thereafter, on additional fault displacement, the rupture bifurcates and fault deformation localizes upon

these two distinct strands, one at each foundation side. Observe the soil heave formation next to the top right caisson corner due to *F1* and the scarp formed at the soil surface due to the emergence of *F2* for h = 3.5 m.

Comparison between the analytically computed and the experimentally deduced shear strain contour plots (Figure 3b and 3c) demonstrates the effectiveness of the numerical method in successfully predicting the generation and evolution of the different fault mechanisms for the whole studied range of fault displacements.

Normal Fault Rupture at s/B = 0.28 (Test ML-08)

This test, wherein the caisson was subject to normal type fault rupture at s = 0.28 B, gave the most intriguing fault–caisson interaction mechanisms and subsequently caused the comparatively most intense caisson response.

Figure 4a displays a set of the centrifuge model test images, captured at different levels of fault displacement, and demonstrates a progressive type of failure associated with the interplay between different failure mechanisms. First, for h = 0.6 m, the caisson acting as a kinematic constraint forces the rupture to deviate significantly from its free field path, actually changing orientation, and to propagate towards the hanging-wall (right) caisson edge. Interestingly, *F1* propagates at a dip angle greater than 90° (about 98°) contradicting the orientation of rupture in the bedrock.

Shear stresses develop along the right sidewall of the caisson and its consequent clockwise rotation causes active type stress conditions to take place on the other (left, footwall) side of the caisson. An

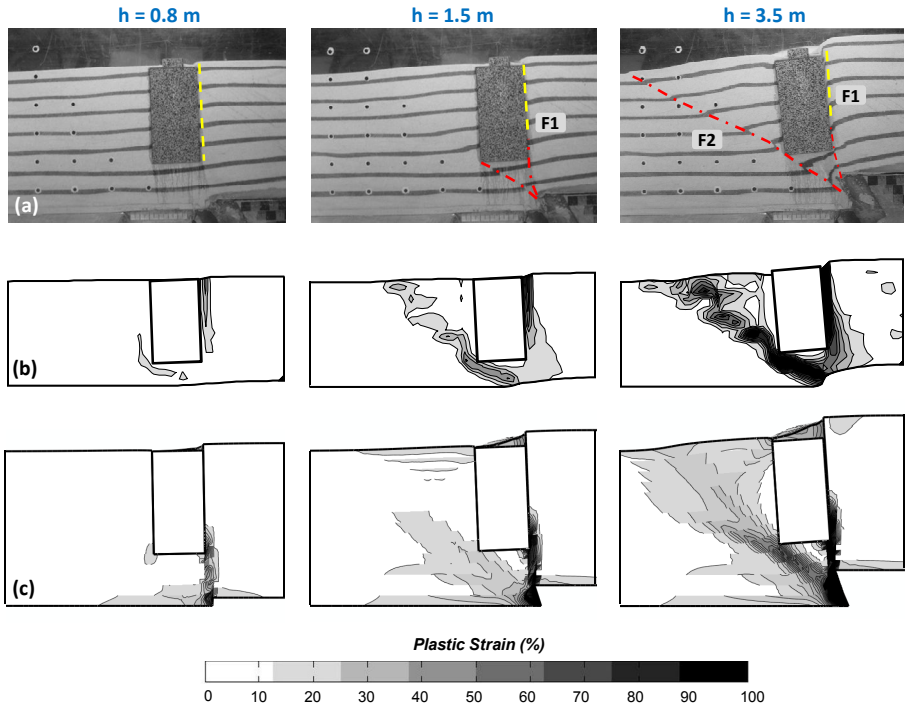

Figure 3. ***Reverse*** **Fault rupture–caisson interaction at different stages of faulting for s/B = 0.22 (Test ML_05): (a) centrifuge test model images; (b) contours of shear strains developed within the soil in the centrifuge test compared to (c) the corresponding numerical analysis.**

active failure wedge forms on the footwall side of the foundation for h = 1.0 m, clearly indicated by the respective shear strain contours in Figure 4b. Soil failure on this side, as well as the soil distress underneath the foundation base due to its significant rotation, "facilitate" the diversion of the rupture to the left of the caisson and a secondary rupture plane (*F2*) is mobilized. Thereafter, a rather subtle interaction mechanism is observed, involving the formation of active and passive failure wedges on the left(footwall) and right (hanging-wall) side of the caisson respectively, and fault propagation on both sides concurrently (see image for h = 2.0 m and the equivalent shear strain contours). Moreover, a sliding plane evidently forms along the left sidewall (highlighted in Figure 4a) and a large gap appears at the top left caisson side.

The numerically computed shear strain contours shown in Figure 4c indicate that the numerical analysis captures the previously described fault rupture–caisson interaction mechanisms closely, demonstrating excellent agreement with the experiment.

Regarding the caisson response, the extensive soil failure around the caisson, owing to the fault deformation spreading on both sides, provoked significant displacements in both the presented tests (Figure 5). The figure indicates the very satisfactory agreement between analysis and experiment throughout the whole range of the examined fault displacements and for both types of tectonic movement. In the particularly destructive case of normal faulting at s/B = 0.28 (Test ML-08), the rotation of the caisson , reaching about 12° for h = 2.5, exceeded by a factor of more than two the rotation experienced in the other two normal fault tests. This indicated the determinative role of the exact caisson position on the prevailing fault–caisson interaction mechanisms and the subsequent caisson response and motivated the following parametric investigation of the effect of the parameter s.

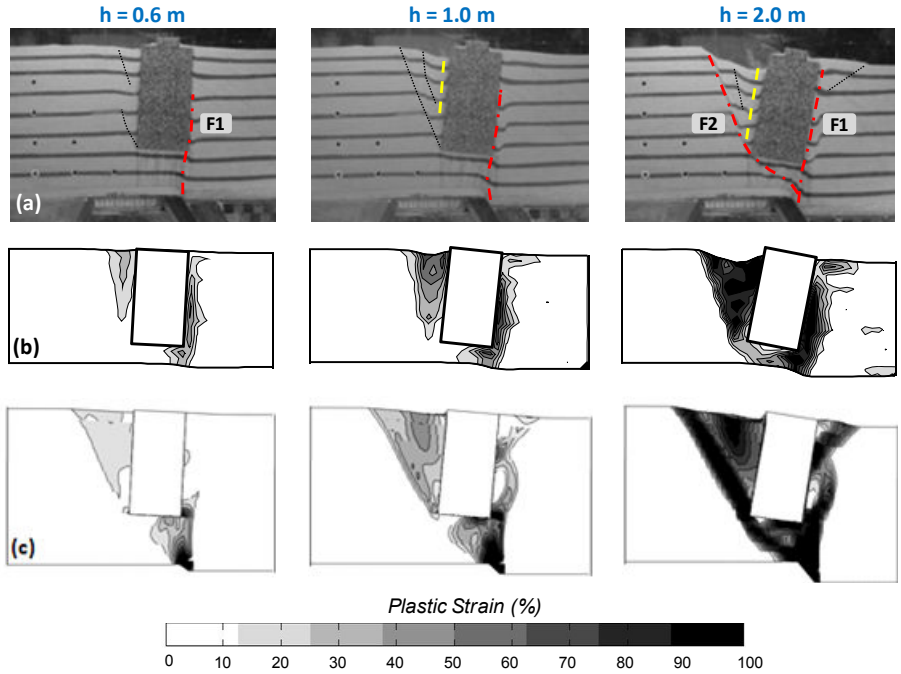

Figure 4. ***Normal*** **Fault rupture–caisson interaction at different stages of faulting for s/B = 0.28 (Test ML_08): (a) centrifuge test model images; (b) contours of shear strains developed within the soil in the centrifuge test compared to (c) the corresponding numerical analysis.**

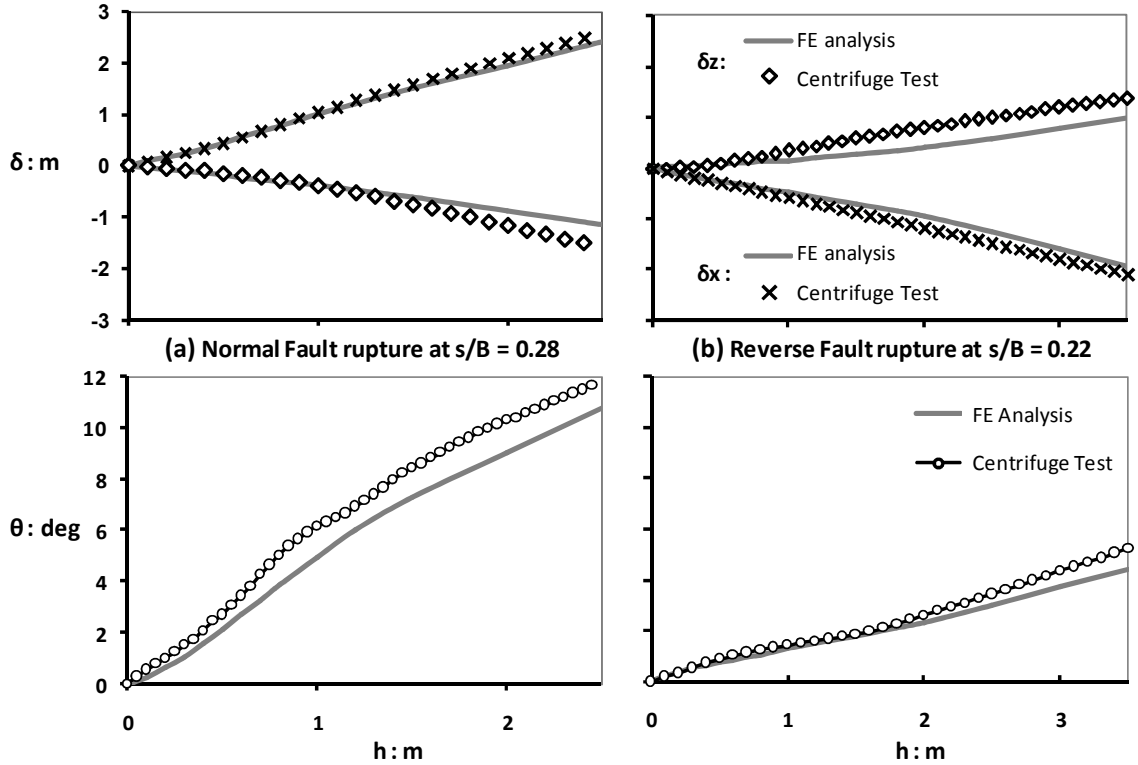

Figure 5. **Comparison between experimental and analytical results in terms of the caisson translational (*δ*) and rotational (*θ*) response with respect to the applied fault throw (*h*).**

FAULT–CAISSON INTERACTION MECHANISMS IN RESPECT OF THE EXACT CAISSON POSITION : PARAMETRIC INVESTIGATION

Gaining enough confidence in the effectiveness of the numerical method in modelling the mechanisms of fault–caisson interaction allowed the conduction of a thorough parametric investigation of the exact caisson position effect on the caisson response. Figures 6 and 7 summarize the results for reverse and normal faults respectively in terms of the caisson displacements (δ_x, δ_z, θ) experienced at different relative fault–caisson positions *s/B* for different levels of fault throw h. The different failure mechanisms taking place are also indicated by the shear strain finite element contours that correspond to different points (positions) in the graph.

For both types of tectonic movement the plane of caisson response with respect to relative position can be divided into three zones of response A,B, and C, broadly representing three different patterns of fault–caisson interaction mechanism and hence three different modes of foundation response. These are illuminated in the following. To allow comparison with the experiments and show the generally good agreement between analytical and experimental results, centrifuge test results are also indicated (with marker points) for the same throws values.

Reverse Fault Rupture–Caisson Interaction Mechanisms

Three different interaction mechanisms can be identified, dividing the graphs of Figure 6 in three zones : (a) Mechanism A, for $s/B < -0.5$; (b) Mechanism B, for $-0.5 \leq s/B < 0.7$; and (c) Mechanism C, for $s/B \geq 0.7$. More specifically:

Mechanism A (−0.5 ≤ s/B < 0.7; i.e. s < −2.5 m since B = 5 m) is observed when the fault rupture interacts with the upper half of the caisson right sidewall. The rupture is diverted towards the hanging wall and the caisson remains on the footwall. As a result, it experiences limited distress, being subjected to relatively small rotational and horizontal displacement, and practically zero uplift. This zone of *s/B* is clearly the most favourable for the performance of the supported structure.

Mechanism B (−0.5 ≤ s/B < 0.7 ; i.e. −2.5 m ≤ s < 3.5 m) occurs when the free field rupture crosses the caisson near its right base corner, as in the case of the previously discussed test ML-05 (*s/B* = 0.22). Fault

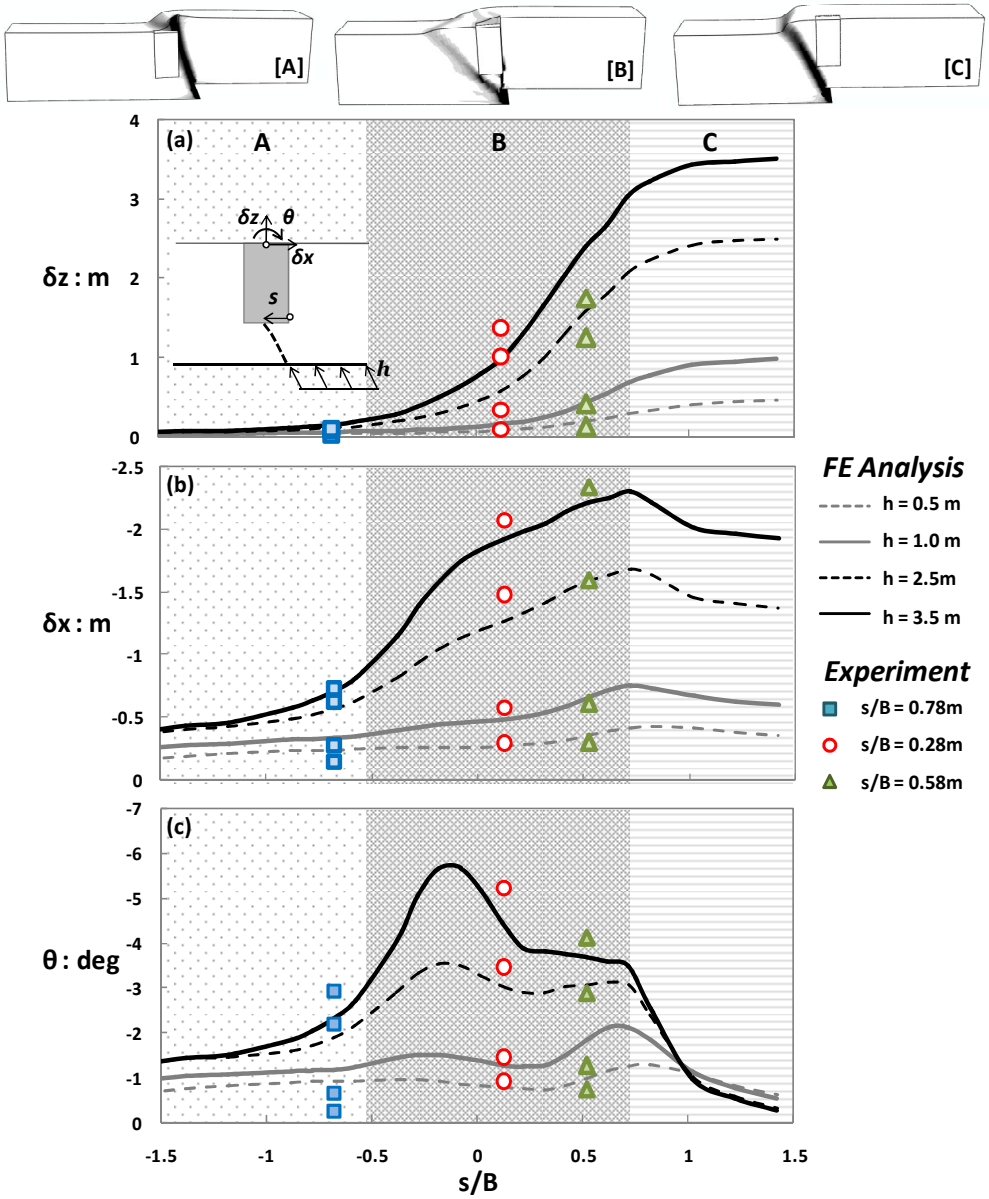

Figure 6. The effect of the exact caisson location (*s*) on the mechanisms of fault rupture–caisson interaction and the consequent caisson response for the case of *reverse* tectonic movement: (a) vertical displacements, (b) horizontal displacements, and (c) rotation for different levels of throw.

bifurcation is observed and deformation occurs simultaneously upon two fault strands, one on each side of the caisson. Increased rotations, and hence horizontal displacements, are associated with this zone of response primarily due to the fault deformation spreading within a wider soil area on both sides of the foundation.

Mechanism C (s/B ≥ 0.7; i.e. s > 3.5 m) the fault rupture diverts towards the caisson footwall side, intersecting at its left base corner. This leads to an abrupt decrease of θ, which is virtually eliminated for $s/B > 1.0$ (i.e. when there is practically no interaction of the fault rupture with the caisson). The caisson experiences pure translational displacement, moving along with the hanging wall.

***Normal* Fault Rupture–Caisson Interaction Mechanisms**

In the same way as with reverse faults, three modes of response can be identified (Figure 7):
Mechanism A (s/B < −0.4; i.e. s < −2 m) takes place when the fault rupture "grazes" the hanging-wall (right) sidewall of the caisson, missing its base by 2 m or more. The rupture path is refracted on the rigid sidewall and deviated towards the hanging-wall (to the right). The caisson remains on the footwall side of the fault, and experiences limited distress for all levels of fault throw h. This is presumably the most favourable area of possible caisson positions.

Mechanism B (−0.4 ≤ s/B < 0.6 ; i.e. −2 m ≤ s < 3 m) is prevalent when the fault rupture crosses the caisson body near its right base corner. As discussed previously for test ML-08 (s/B = 0.28), the interaction of the caisson with the fault rupture is in this case quite complex, involving : (i) bifurcation of the shear zone along both sides of the caisson, (ii) formation of an active failure wedge at the footwall (left) side of the caisson due to its substantial rotation, and (iii) formation of a passive-type failure wedge at the hanging-wall (right) side of the caisson (also due to the rotation). This area of possible interaction positions, is probably the most detrimental for the system response.

Mechanism C (s/B ≥ 0.6; i.e. s > 3 m) prevails when the fault rupture crosses the caisson close to its footwall (left) corner, or misses it completely on the footwall (left) side. The rupture is diverted towards the footwall and the caisson translates downwards, following the hanging wall, with only minor rotation

CONCLUSIONS

This paper has presented a combined experimental and numerical study of the interaction between a dip slip fault rupture, the soil, and an embedded rigid caisson foundation. The key conclusions can be summarized as follows :

(a) Caisson foundations interact with dip-slip fault rupture (normal and reverse) and change sometimes dramatically its free field path. The rigid caisson body acts as a kinematic constraint, which forces the fault to divert. This is an important difference of caissons compared to other types of foundations (shallow footings or piles), which can only cause partial fault deviation if at all.

(b) The numerical method was validated through successful comparisons with centrifuge test results, revealing its effectiveness in capturing qualitatively and quantitatively the mechanisms of fault rupture–caisson interaction. This gives confidence that the same method can be used to study other similar problems or be used as a design tool.

(c) The validation of the numerical method allowed the conduction of a parametric study to further investigate the effect of the exact foundation position, which proved to be a determinative parameter controlling the response of the system. The different FR-SFSI mechanisms taking place at different positions s/B were identified and the consequent foundation performance was discussed.

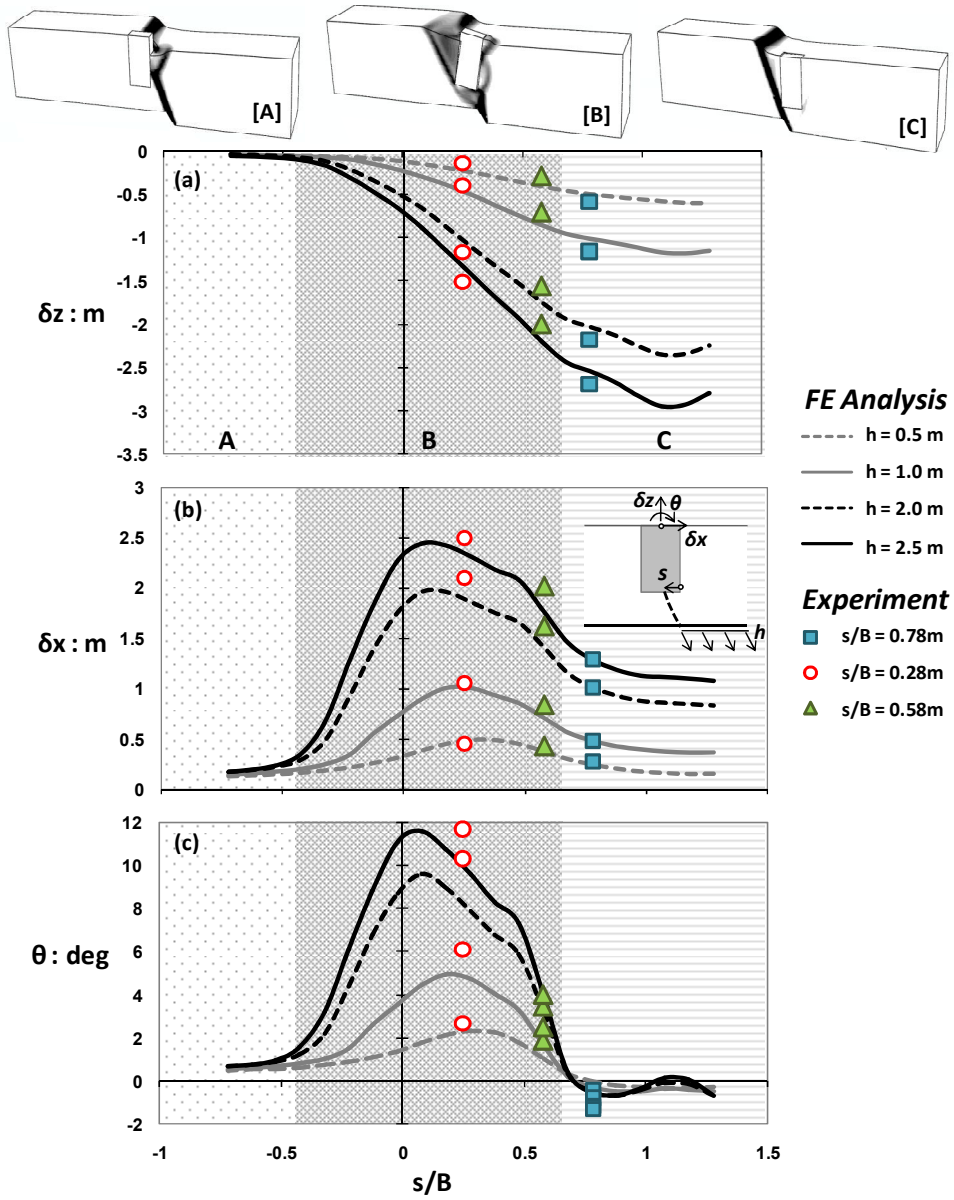

Figure 7. The effect of the exact caisson location (*s*) on the mechanisms of fault rupture–caisson interaction and the consequent caisson response for the case of *reverse* tectonic movement: (a) vertical displacements, (b) horizontal displacements, and (c) rotation for different levels of throw.

AKNOWLEDGEMENTS

NTUA authors would like to acknowledge financial support from the EU 7th Framework research project funded through the European Research Council's Programme "Ideas", Support for Frontier Research – Advanced Grant, under Contract number ERC-2008-AdG 228254-DARE.

REFERENCES

Ahmed, W. & Bransby, M.F. (2009). The interaction of shallow foundations with reverse faults. *Journal of Geotechnical and Environmental Engineering* 135, No. 7, 914-924.

Anastasopoulos, I. & Gazetas G. (2007). Foundation-Structure Systems over a Rupturing Normal Fault: Part I. Observations after the Kocaeli 1999 Earthquake. *Bulletin of Earthquake Engineering*, 5, No. 3, 253–275.

Anastasopoulos, I. Gazetas, G. Bransby, M.F. Davies, M.C.R. & El Nahas, A. (2007). Fault Rupture Propagation through Sand : Finite Element Analysis and Validation through Centrifuge Experiments. *Journal of Geotechnical and Geoenvironmental Engineering*, ASCE, 133, No. 8, 943–958.

Anastasopoulos, I. Gazetas, G. Bransby, M.F. Davies, M.C.R. & El Nahas, A. (2009a). Normal Fault Rupture Interaction with Strip Foundations. *Journal of Geotechnical and Geoenvironmental Engineering, ASCE*, 135, No. 3, 359-370.

Bransby, M.F. Davies, M.C.R. El Nahas, A. & Nagaoka, S. (2008a). Centrifuge modelling of normal fault-foundation interaction. *Bulletin of Earthquake Engineering*, 6, No. 4, 585-605.

Bransby, M.F. Davies, M.C.R. El Nahas, A. & Nagaoka, S. (2008b). Centrifuge modelling of reverse fault-foundation interaction. *Bulletin of Earthquake Engineering*, 6, No. 4, 607-628.

Chang, K-C. Chang, D-W. Tsai, M-H. & Sung, Y-C. (2000). Seismic performance of highway bridges. *Earthquake Engineering and Engineering Seismology*, 2, No. 1, 55-77.

Dong, J.J. Wang, C.D. Lee, C.T. Liao, J.J. & Pan, Y.W. (2003). The influence of surface ruptures on building damage in the 1999 Chi-Chi earthquake: a case study in Fengyuan City. *Engineering Geology*, 71, 157–179.

Faccioli, E. Anastasopoulos, I. Callerio, A. & Gazetas, G. (2008). Case histories of fault–foundation interaction. *Bulletin of Earthquake Engineering*, 6, 557–583.

Gaudin, C. (2002). *Modelisation physique et numerique des ecrans de soutenement: application a l'etude de l'effet d'une surcharge sur le sol soutenu*. PhD. thesis, Universite de Nantes.

Loli, M. Bransby, M.F. Anastasopoulos, I. Gazetas, G. (2010a). Interaction of Caisson Foundations with a Seismically Rupturing Normal Fault : Centrifuge Testing versus Numerical Simulation. *Geotechnique*, submitted for publication.

Loli, M. Anastasopoulos, I. Bransby, M.F. Ahmed, W. Gazetas, G. (2010b). Caisson Foundations subjected to Reverse Fault Rupture : Centrifuge Testing and Numerical Analysis. *Journal of Geotechnical and Geoenvironmental Engineering*, ASCE, submitted for publication.

Pamuk, A. Kalkan, E. & Ling, H.I. (2005). Structural and geotechnical impacts of surface rupture on highway structures during recent earthquakes in Turkey. *Soil Dynamics & Earthquake Engineering*, 25, No. 7-10, 581-589.

Paolucci, R. & Yilmaz, M.T. (2008). Simplified theoretical approaches to earthquake fault rupture–shallow foundation interaction. *Bulletin of Earthquake Engineering*, 6, No. 4, 629-644.

Ulusay, R. Aydan, O. & Hamada, M. (2002). The behaviour of structures built on active fault zones: examples from the recent earthquakes of Turkey. *Structural Engineering & Earthquake Engineering*, JSCE, 19, No. 2, 149-167.

White, D.J. Take, W.A. & Bolton, M.D. (2003). Soil deformation measurement using particle image velocimetry (PIV) and photogrammetry. *Geotechnique*, 53, No. 7, 619-631.

Yilmaz, M.T. & Paolucci, R. (2007) "Earthquake fault rupture–shallow foundation interaction in undrained soils." *Earthquake Engineering and Structural Dynamics*, **36**, No. 1,101–118.

Youd, T. L. Bardet, J.P. & Bray, J.D. (2000). Kocaeli, Turkey, Earthquake of August 17, 1999 Reconnaissance Report. *Earthquake Spectra*, Suppl. A to 16, 456.